PHYSICAL REVIEW E **89**, 012811 (2014)

Potential for the dynamics of pedestrians in a socially interacting group

Francesco Zanlungo,* Tetsushi Ikeda, and Takayuki Kanda
IRC-ATR, Kyoto, Japan & JST CREST, Tokyo, Japan

(Received 13 September 2013; revised manuscript received 29 November 2013; published 22 January 2014)

We introduce a simple potential to describe the dynamics of the relative motion of two pedestrians socially interacting in a walking group. We show that the proposed potential, based on basic empirical observations and theoretical considerations, can qualitatively describe the statistical properties of pedestrian behavior. In detail, we show that the two-dimensional probability distribution of the relative distance is determined by the proposed potential through a Boltzmann distribution. After calibrating the parameters of the model on the two-pedestrian group data, we apply the model to three-pedestrian groups, showing that it describes qualitatively and quantitatively well their behavior. In particular, the model predicts that three-pedestrian groups walk in a V-shaped formation and provides accurate values for the position of the three pedestrians. Furthermore, the model correctly predicts the average walking velocity of three-person groups based on the velocity of two-person ones. Possible extensions to larger groups, along with alternative explanations of the social dynamics that may be implied by our model, are discussed at the end of the paper.

DOI: 10.1103/PhysRevE.89.012811 PACS number(s): 89.65.Ef, 05.10.−a, 89.20.−a, 89.75.−k

I. INTRODUCTION

A. Motivation

The purpose of this work is to develop a dynamical model for the relative motion of pedestrians in groups. Social groups represent an important component of urban crowds [1–3], reaching in some environments up to 85% of the walking population [4]. Nevertheless, until recent times almost all microscopic crowd dynamics models used independent pedestrians as a basic unit, completely ignoring the effects of the intergroup interaction. The presence of groups definitely has a large impact on crowd dynamics, influencing macroscopic behavior (density-velocity diagrams and escape times) in both the medium- and high-density regimes. In the past few years many works studied this problem [5–10], bringing new insight to the simulation of realistic pedestrian crowds. We nevertheless believe that the dynamics of free-walking socially interacting groups (i.e., in the low-density regime) has still not been deeply investigated. While the field of proxemics [11,12] has been largely studied for standing-still pedestrians, the analysis of the relative position of unconstrained walking social groups [13,14] has been quite limited, and a comprehensive dynamical model is still missing. In this work we show that, at least in the low-density regime, the very fact that pedestrians are socially interacting (and thus arguably feel a very similar influence from the *external field*, i.e., the environment) enables using statistical mechanics methods to compare the observed pedestrian behavior with the one predicted by the proposed potential. We thus think that this work may also be an interesting contribution to the growing field of statistical physics of social dynamics [15].

B. Physical models in pedestrian dynamics

The application of physical models to social sciences, in particular using statistical physics methods, has a long history and nowadays involves many fields, including opinion, cultural, and language dynamics [15]. A field in which physical models have been widely used is the dynamics of pedestrians crowds. The first models of the crowd used methods coming from fluid dynamics [16], an approach that has been further developed and is still in use [17]. Nevertheless, such an approach does not allow us to describe the microscopic behavior of individuals and to account for the diversity of the pedestrians in the crowd. A possible way to account for a microscopic dynamics is to use cellular automata [18–20], while, by introducing a continuous space dynamics, it is possible to use interaction forces and describe the pedestrians as particles of a many-body mechanical system.

Indeed the social force model (SFM) [21] describes the behavior of pedestrians through a system of second-order differential equations, in which the particle accelerations are given by forces accounting for the social and physical interactions in the crowd. The model has been shown to reproduce qualitatively and quantitatively many aspects of crowd behavior, in particular those connected to egress and panic situations, which are of undeniable social interest [22–24]. Initially, the model tried to describe mainly physical interaction and short-distance collision avoidance, using repulsive forces depending only on the relative distance between pedestrians, but then, to properly describe the collision avoidance of pedestrians at various densities, specifications of the model using forces based also on relative velocities have been introduced [25,26]. Despite these successes, the connection between the forces of the SFM and the actual microscopic dynamics of pedestrians has not been deeply investigated or demonstrated, and attempts at a rigorous analysis of the physics implied by the equations are limited to unrealistic settings [27]. Some works have suggested that a force-based approach is too simplistic to describe human collision avoidance and have proposed methods based on local path planning [28,29].

The reason for this lack of testing between the dynamics implied by the equations and the microscopic behavior of real pedestrians originates obviously from the lack of reliable data. Models can be calibrated on controlled experiments [26,30,31] or on real-world data [32]. While the first approach may be biased by the unnatural behavior of humans in these

*zanlungo@atr.jp

experiments, the second one is limited not only by increased measurement noise but mainly by the lack of knowledge of the pedestrians' internal dynamics (their motivations).

When studying a walking socially interacting group in a situation in which collision avoidance is negligible, we may assume, given the similar motivations of the members of the group, that the influence of the environment on them is almost the same. The dynamics due to such an *external field* may then be subtracted in the group center-of-mass frame. As we show, this allows a direct comparison of the physics described by the model and the actual pedestrian behavior (at least from a statistical point of view).

C. Behavior of walking groups

1. Empirical observations

Social groups are defined in Ref. [33] as groups of people who are engaged in a social relation to one or more pedestrians and move together towards a common goal. The term *relation* refers to oral communication possibly accompanied with nonverbal elements such as body language, gestures, or exchange of gaze [34]. In particular, *eye contact* is an essential nonverbal factor that helps in estimating the reactions of the partners and in anticipating their actions [35]. It is also suggested that eye contact affects the equilibrium of physical proximity [36].

The spatial relationship of socially interacting people, i.e., proxemics, has been largely studied, starting from the seminal works of Refs. [11] and [12] in which the relative distance and spatial distribution of people participating in social activities are investigated, but most studies focused on people standing still. References [5] and [13] are among the first studies to report observations (based mainly on camera recordings) of the behavior of walking groups. While Ref. [5] reports that the spatial structure of a freely walking (i.e., not environmentally constrained) n pedestrian group is a line of abreast-walking pedestrians that tends to be bent into "V" or "U" formations (i.e., the pedestrians on the wings walk ahead) when the crowd density grows, Ref. [13] reports different spatial structures, suggesting, for example, that the V configuration is the most common one for three-person groups (regardless of crowding) and that larger groups tend to split into smaller subgroups. Nevertheless, Ref. [13] does not analyze the possible effects of environmental constraints on the observed behaviors (the width of the sidewalks pedestrians were observed in was comparable to the group spatial sizes), and neither provides a quantitative study of 2D space structures, nor follows groups for a time interval long enough to analyze their change in time. To automatically track pedestrians, Ref. [37] models the distance between them as a Rice distribution with a maximum around $\approx$0.7–0.8 m and a normal (von Mises) distribution of angles around the abreast configuration.

In Ref. [14], whose empirical observations are largely reported in this work, we use laser range finders along with camera recordings to analyze the spatial and time stability of social group formations. We study the empirical probability distribution of pedestrian positions in the group center-of-mass reference frame (after aligning the orientation of the frame with the group velocity) and say that an n pedestrian group has a stable (i.e., largely prevalent in time and over groups) formation if the pedestrian position *pdf* presents exactly n clear maxima. We find that two-pedestrian groups have a stable abreast formation with a distance between the pedestrians of $\approx$0.75 m, while three-pedestrian ones have a stable V formation, with a central angle of $\approx 150^\circ$, even when walking unconstrained. For larger groups, we do not find any stable overall configuration, unless we divide the groups into two- or three-person subgroups, which are more stable in space and time.

In a different environment (the German Protestant Church Congress in Dresden), and with a different method (observation from top view cameras, for a relatively short time), Ref. [4] finds for two- and three-pedestrian groups one-dimensional (1D) and two-dimensional (2D) observable distributions very similar to those of Ref. [14]. For four-pedestrian groups, they find a U formation.

2. Models

While social groups represent an important component of pedestrian crowds [1–3], their impact on crowd dynamics has been largely overlooked in simulation models until recent times. The authors of Ref. [5] extended the social force model to describe the dynamics of such groups and their effect on the crowd flow, proposing a dynamical model that describes an abreast formation for freely walking pedestrians, a formation that bends at higher densities.

In the last years other models to simulate the dynamics of groups in a crowd have been proposed, focusing mainly on the effect of the presence of groups on egress dynamics. The authors of Ref. [6] introduce a rule model with two proxemics distances, a minimum distance towards pedestrians outside the group and a maximum one towards pedestrians in the group, while Ref. [7] postulates attractive exponential bonds along the relative position vector; but these two aforementioned works do not pay attention to the group configuration. The authors of Ref. [8] assume an abreast condition for freely walking groups as part of their cellular automata model, as does Ref. [9], which studies in continuous space the transition to V or "riverlike" formations to avoid obstacles. The authors of Ref. [10] assume that three-person groups may have collision-free V formations to facilitate communication and describe them through a three-person specific parameter.

Among these works, only Ref. [5] validates results comparing to microscopic free walking configurations, and, according to our knowledge, no previous work describes the group dynamics introducing a 2D discomfort potential, providing an analytical and numerical study of its consequences and determining the structure and velocity of three-person groups on the basis of two-person ones, as we do in the present work.

D. Plan of the paper

In Sec. II we propose a model for the dynamics of the relative position of two pedestrians in a group. We conjecture that the position of *each pedestrian*[1] is determined by a potential that represents the discomfort that the pedestrian

[1]The discomfort of each pedestrian is determined by a different potential. See the discussion in Sec. II C.

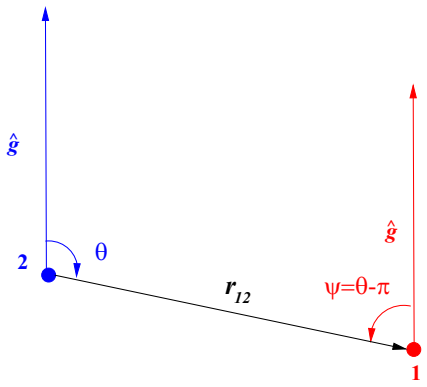

FIG. 1. (Color online) $\mathbf{r}_{ij}$ and $\hat{\mathbf{g}}$ for a two-pedestrian system. r and θ give the position of pedestrian 1 with respect to 2 in the $\hat{\mathbf{g}}$ oriented frame. $|\theta|$ is the angle that 2's gaze has to span between the goal and 1. The corresponding angle for 1 is given by $|\psi|$. In the figure, $\theta > 0$ and $\psi < 0$.

feels when interacting at a given position. We assume that the pedestrian accelerations are determined by the negative gradient of the potential, i.e., that the motion of the pedestrians is aimed to maximize their comfort. The main properties of the resulting equations for the motion of the pedestrians are then analyzed.

In Sec. III we describe our data collection method and the quantitative results of our observations relating the probability distribution for the positions of pedestrians in a group and group velocities. In Sec. IV we compare the observed 2D probability distribution of the relative position of pedestrians in a two-person group with the Boltzmann distribution determined by the proposed potential and use this comparison to calibrate the model's parameter.

In Sec. V we develop a simulator for the two-person system and compare its results to the empirical ones of Sec. III and to the analytical ones of Sec. IV. In Sec. VI we study three-person groups assuming first-neighbor interaction. We first derive some analytical results for the equilibrium configuration and then use our simulator to analyze the behavior that the model predicts for these groups and compare the results to empirical observations. We also provide a simultaneous calibration of the model on two- and three-pedestrian group data and discuss addition of second-neighbor terms to improve the model's capability of reproducing empirical data.

In Sec. VII we discuss the extension to larger groups, and in Sec. VIII we analyze possible different interpretations of the behavior described by our equations and discuss the achievements and limitations of our work.

II. TWO-PEDESTRIAN MODEL

A. Description of the model

We derive the *discomfort potential* for pedestrians involved in a social interaction, as a function of the angle θ between the relative distance vector $\mathbf{r}$ and the common goal direction and of the distance r (see Fig. 1). θ is related to the angle that the pedestrian's gaze has to span to focus on the walking direction and on the partner position. We assume that r and θ independently determine the pedestrian discomfort, each one with a different weight, C_r and C_θ. These two parameters, along with the preferred distance for social interaction, r_0, determine the probability distribution of the relative position in a two-pedestrian group. A fourth parameter, η, is related to the tendency of pedestrians to walk ahead or behind their partner. We show that η does not affect the probability distribution of relative position in two-pedestrian groups but modifies the group velocity. In particular, $\eta < 0$ causes pedestrians in groups to walk slower. The presence of the parameter η allows us to derive the velocity and the configuration of three-person groups from the two-person ones and if $\eta < 0$ the three pedestrians walk in a V formation with the central one on the rear (three-person group results are derived in Sec. VI). In Sec. VIII we discuss how $\eta < 0$ can be interpreted as a way to express in a mathematical form the "cognitive load" of social interaction that causes pedestrians to walk slower.

B. Definitions and assumptions

Let us consider n pedestrians with positions $\mathbf{r}_i$ and velocities $\mathbf{v}_i$ in an *environment reference frame*,[2] walking towards a common goal, whose direction is given by a unit versor $\hat{\mathbf{g}}$. We define the preferred velocity vector of the pedestrians as $\mathbf{v}_p = v_p\hat{\mathbf{g}}$.[3]

According to the SFM framework, the differential equation for the motion of pedestrian i is

$$\dot{\mathbf{v}}_i = \mathbf{F}_i^g + \sum_{j\in n, j\neq i} \mathbf{F}_{ij} + \mathbf{F}_i^c + \mathbf{F}_i^e + \boldsymbol{\xi}_i. \tag{1}$$

Here

$$\mathbf{F}_i^g = \frac{(\mathbf{v}_p - \mathbf{v}_i)}{\tau} \tag{2}$$

is a drag force towards the goal,[4] $\mathbf{F}_{ij}$ is the interaction force with the group partner j, while $\mathbf{F}_i^c$ stands for the force determined by collision avoidance towards pedestrians outside the group and other obstacles. $\mathbf{F}_i^e$ gives all the other interactions with the environment and $\boldsymbol{\xi}_i$ is a white noise term representing the pedestrian's internal dynamics.[5]

We define the center-of-mass position and velocity as

$$\mathbf{X} = \frac{\sum_{i=1}^n \mathbf{r}_i}{n}, \qquad \mathbf{V} = \frac{\sum_{i=1}^n \mathbf{v}_i}{n}, \tag{3}$$

and name the positions and velocities in the center-of-mass system $\mathbf{r}_i^{\text{c.m.}}$, $\mathbf{v}_i^{\text{c.m.}}$. We assume that $\mathbf{F}_i^e$ may be written as drag force as in Eq. (2) and determines basically a redefinition of the pedestrian (sub-)goals, which may be time dependent (determined by the navigation path towards the final goal,

[2] An arbitrarily oriented frame in which walls and similar architectural elements have zero velocity.

[3] $\hat{\mathbf{g}}$ and v_p are considered equal for all group members.

[4] τ is the time scale to recover the preferred velocity, whose value is $\approx$0.66 s according to Ref. [26].

[5] As shown by Eq. (1), the term force has to be intended purely with the meaning of "behavioral interaction," i.e., we consider situations in which the actual physical interactions are absent or negligible, and all masses are equal to 1 and dimensionless. Forces have thus the dimensionality of accelerations.

influenced by diverse environment features [38–41]) but are assumed equal for socially interacting pedestrians. The collision term is pedestrian dependent, but we assume that at low pedestrian densities ($\rho \ll 1$ pedestrian per square meter), and when studied over a long-enough time scale, it can be approximated as a white-noise term.

Based on these considerations, from a statistical point of view, i.e., if the consequences of such a dynamics are studied over long-enough times, the dynamics of the pedestrian is given by

$$\dot{\mathbf{v}}_i = \frac{\tilde{\mathbf{v}}_p - \mathbf{V}}{\tau} - \frac{\mathbf{v}_i^{\text{c.m.}}}{\tau} + \sum_{j\in n,\ j\neq i} \mathbf{F}_{ij} + \boldsymbol{\Xi}_i, \tag{4}$$

where $\tilde{\mathbf{v}}_p$ includes the redefinition of the (sub-)goal and the white noise term $\boldsymbol{\Xi}_i$[6] accounts for $\boldsymbol{\xi}_i$ and for collision avoidance.

Let us now consider a two-pedestrian system and the dynamics of its relative variables

$$\mathbf{r} = \mathbf{r}_1 - \mathbf{r}_2, \quad \mathbf{v} = \mathbf{v}_1 - \mathbf{v}_2, \tag{5}$$

defining

$$\mathbf{f} = \mathbf{F}_{12} - \mathbf{F}_{21}, \tag{6}$$

we obtain

$$\dot{\mathbf{v}} = -\frac{\mathbf{v}}{\tau} + \mathbf{f} + \boldsymbol{\Xi}. \tag{7}$$

If we assume that $\mathbf{f}$ may be derived from a potential U and that the effect of the purely dissipative term $-\mathbf{v}/\tau$ combined with the white noise $\boldsymbol{\Xi} = \boldsymbol{\Xi}_1 - \boldsymbol{\Xi}_2$ may be treated as a thermal bath, then the statistical properties of $\mathbf{r}$ are determined by the potential U (see Appendix A for the definition of statistical observables).

C. Non-Newtonian terms

In deriving Eq. (7) we restricted ourselves to the reference frame comoving with the center of mass of the system. The reason for doing that is mainly operative, since, as we will see in Sec. III, all our observables are defined in such a frame, with the obvious exception of the group velocity, i.e., the velocity of the center of mass, that is defined in the environment frame. Nevertheless, an important distinction between the nature of the force $\mathbf{F}_{ij}$ of Eq. (1) and the usual internal forces of a physical system has to be stressed. In Newtonian mechanics, when the interaction between particles is described by an action-at-distance force, the closed system is considered as translation invariant, i.e., the corresponding potential assumes the form $U(\mathbf{r}_i - \mathbf{r}_j)$, from which Newton's third law of dynamics, $\mathbf{F}_{ij} = -\mathbf{F}_{ji}$, and momentum conservation may be derived. In such a case, in Eq. (6) we have $\mathbf{f} = 2\mathbf{F}_{12}$ and the relative force is obviously obtained by same the potential U that determines the internal forces.

When describing pedestrian interaction using a system of forces, the action-reaction principle may not apply. A classical example is the problem of vision, which creates an asymmetry between the interacting pedestrians.[7] For example, Ref. [27] studied the effect of a sharp cone of vision in a classical repulsive interaction potential [collision avoidance only towards the particles (pedestrians) that fall in the cone], while in Ref. [5] the aligning potential acts only on the pedestrians that are ahead of the group, i.e., that have the center of mass of the group out of their vision field. Similar non-Newtonian forces generate an acceleration of the center of mass (with respect to the environment frame in which the forces are defined) due to internal forces. Such an acceleration may operate on Eq. (2) and lead to different velocities for pedestrian groups with respect to single pedestrians (as empirically observed and reported in Table I).

TABLE I. Number of pedestrian groups N for different group size n, along with average velocity $\langle v\rangle$, standard deviation σ_v, and standard error σ_v^e (in mm/s), and overall trajectory point number S. Only data points in which all pedestrians have velocities larger than 0.5 m/s were used.

	$n=1$	$n=2$	$n=3$	$n=4$
N	9495	854	102	13
$\langle v\rangle$	1336	1159	1112	1074
σ_v	197	173	165	138
σ_v^e	2	6	16	40
S	712052	70513	8721	893

Since we want our model to be able to describe such non-Newtonian terms, we cannot use a single potential in the form $U(\mathbf{r}_i - \mathbf{r}_j)$ to describe the two-pedestrian system in the environment frame. As we show below, the problem may be solved by using a different potential, or *discomfort function* (the meaning of the term discomfort will be explained below), to describe the dynamics of each pedestrian. The acceleration due to interaction with group members will be given for each pedestrian by the negative gradient of the discomfort function

$$D_i = \sum_{j\neq i} D_{ij}(\mathbf{r}_i - \mathbf{r}_j), \tag{8}$$

where D_{ij} is the potential *determining the motion of* i *given the relative distance from* j. We will assume the discomfort of j with respect to i to be given by a function D_{ji} that has the same dependence on the variable $\mathbf{r}$, i.e., $D_{ij}(\mathbf{r}) = D_{ji}(\mathbf{r}) \equiv D(\mathbf{r})$,[8] but we will allow D not to be invariant under inversion, i.e., in principle, $D(\mathbf{r}) \neq D(-\mathbf{r})$. As a consequence, at a given time t, we may have

$$D_{ij}(\mathbf{r}_i(t) - \mathbf{r}_j(t)) \neq D_{ji}(\mathbf{r}_j(t) - \mathbf{r}_i(t)), \tag{9}$$

so the dynamics of the each pedestrian is determined by a different potential and is non-Newtonian.

[6] Assumed to be normally distributed.

[7] Obviously also non-Newtonian terms not related to vision may be introduced; for example, the non-Newtonian term in our model is only implicitly related to vision, since we introduced it on the basis of a "comfort of interaction" principle.

[8] This means that we are considering all pedestrians as equal and indistinguishable.

It is easily verified that in a frame comoving with the center of mass, the dynamics of the system is given by

$$\dot{\mathbf{v}} = \mathbf{f} = -\nabla(D(\mathbf{r}) + D(-\mathbf{r})) \equiv -2\nabla U(\mathbf{r}). \quad (10)$$

The potential U is now manifestly invariant under inversion, so in the noninertial center-of-mass frame the overall momentum is conserved and the potential U may be used to study the statistical properties of the system. As we see below, the non-Newtonian terms have observable effects on the group velocities (and on the three-pedestrian group configuration), resulting in good agreement with empirical observations.

D. Derivation of the potential

Let us assume that the interaction force, acting on pedestrian i as an effect of the presence of j, may be derived by a function $D_{ij}(\mathbf{r}_i - \mathbf{r}_j)$ according to

$$\mathbf{F}_{ij} = -\nabla_i D_{ij}(\mathbf{r}_i - \mathbf{r}_j), \quad (11)$$

where ∇_i stands for derivation with respect to $\mathbf{r}_i$. Analogously, the force on pedestrian j is given by $\mathbf{F}_{ji} = -\nabla_j D_{ji}(\mathbf{r}_j - \mathbf{r}_i)$. As discussed above, we assume the form of the two potentials to be the same, $D_{ij}(\mathbf{r}) = D_{ji}(\mathbf{r})$, but since we allow $D(\mathbf{r}) \neq D(-\mathbf{r})$, we do not drop the subscripts to recall that the motion of each pedestrian is determined by the minimization of a different function.

The force $\mathbf{F}_{ij}$ represents an act (acceleration) that pedestrian i performs as a result of his or her relative position with respect to j. Since such an action is directed to minimize the function D_{ij}, and assuming that the spatial interaction towards the partner is aimed to reach the most comfortable configuration for social interaction, we may name the function D_{ij} as the *discomfort function* or *discomfort potential*[9] of i due to its location with respect to j, i.e., as a mathematical way to represent that the pedestrian is not located in an optimal location for social interaction and will perform an act (acceleration) to proceed towards a better location. The minima of D_{ij} will thus represent relative locations in which i attains maximum comfort for social interaction with j.[10]

For walking and interacting pedestrians we expect D_{ij} to depend on the relative position $\mathbf{r}_{ij} \equiv \mathbf{r}_i - \mathbf{r}_j$ and on the versor $\hat{\mathbf{g}}$, and we seek an expression in the form $D(r,\theta)$, where $r = |\mathbf{r}_{ij}|$ and θ is the angle between $\mathbf{r}_{ij}$ and $\hat{\mathbf{g}}$ (see Fig. 1).

1. Angular dependence

We define θ to assume values in $(-\pi,\pi]$, so also

$$\psi \equiv \begin{cases} \theta - \pi & \text{if } \theta > 0, \\ \theta + \pi & \text{if } \theta \leqslant 0, \end{cases} \quad (12)$$

assumes values in the same range. If $|\psi|$ gives the angle between the direction to the goal and the direction to pedestrian j from i's point of view, $|\theta|$ is the corresponding angle for j (Fig. 1). The walking pedestrians need to have the direction to the goal $\hat{\mathbf{g}}$ in their field of view, but for social interaction [34] they also need to have the position of their partner reachable to their gaze. The discomfort is then a growing function of the angle $|\psi|$ that their gaze has to span. At the same time, pedestrians want to meet their partner's gaze [35], so the pedestrian's discomfort is also a growing function of the angle the partner's gaze has to span, $|\theta|$. The simplest form that satisfies symmetry under the parity operation $\theta \to -\theta$ is[11]

$$\Theta^{\eta}(\theta) = (1+\eta)\theta^2 + (1-\eta)\psi^2, \quad (13)$$

with $-1 \leqslant \eta \leqslant 1$.

The potential Θ^{η} assumes minima in $\pm(1-\eta)\pi/2$ and is continuous for all θ but has cuspidal local maxima in 0 and π (excluding the case $\eta = \pm 1$ for which one of these points turns into a smooth global minimum). While the potential is symmetric under $\theta \to -\theta$, when $\eta \neq 0$ it is not symmetric under $\theta \to \theta + \pi$ (i.e., under $\theta \to \psi$), and thus the discomfort function is not symmetrical under inversion, $D(\mathbf{r}) \neq D(-\mathbf{r})$. As discussed above, this implies that for $\eta \neq 0$ the force is non-Newtonian and the system's center of mass is accelerated in the environment frame as a result of the sum of internal forces not obeying the third principle of dynamics. As we show in Sec. II F, when $\eta > 0$ the effect of this non-Newtonian term corresponds to an acceleration towards the direction of the goal, causing a higher velocity for two-person groups with respect to individuals, while a negative η leads to an acceleration opposite to $\hat{\mathbf{g}}$, causing groups to move slower than individuals.

Even though our model does not explicitly define a vision field, from the position of the minima we understand that η may be related to this concept. In particular, when $\eta < 0$ pedestrians give a higher discomfort weight to ψ^2 than to θ^2, i.e., they prefer to have the partner in their vision field rather than being in the partner's field, and, as a result, their discomfort function D assumes a minimum with $|\theta| > \pi/2$. On the contrary, if $\eta > 0$, pedestrians try to locate themselves in the partner's field of view (they act as "leaders") and their discomfort is minimized with $|\theta| < \pi/2$. If we assume the discomfort of each pedestrian to be given by the same function, $D_{ij}(\mathbf{r}) = D_{ji}(\mathbf{r})$,[12] then η assumes the same value for both partners, and the two pedestrians may be at the same time in their position of minimum discomfort only if $\eta = 0$. It is this "frustration" that causes the accelerating non-Newtonian term for $\eta \neq 0$.

[9] The term function recalls the difference with the usual meaning of potential in physics, i.e., that each pedestrian in the system is described by a different potential. Nevertheless, since from any other point of view such a function is equivalent to a physical potential, we will use the two terms as interchangeable.

[10] D will be simply called discomfort function, but a more precise term would be *social interaction discomfort function* since pedestrians are in general trying to minimize also social interaction unrelated terms [42].

[11] We stress that such a symmetry is not necessarily true for crowd dynamics [43]. Nevertheless, we assume it to be valid for the angular dependence of the discomfort potential of socially interacting pedestrians.

[12] This assumption, at least for pedestrians who are socially interacting, is justified by our observations of Sec. III that do not clearly show the presence of "leaders" and "followers."

2. Radial dependence

The radial potential has to attain a minimum at the distance that is most comfortable for social interaction, r_0. For $r > r_0$ the potential will be attractive, accounting for the discomfort due to interacting at too-large a distance, while for $r < r_0$ it will be repulsive, accounting for the discomfort of being too close and for the physical constraints.[13] We may assume that when two standing-still pedestrians are far away ($r \gg r_0$) they start walking straight towards each other, with no regard to θ. Furthermore, this behavior should be almost distance independent for large distances (we do not want the force to diverge or fade out for $r \to \infty$[14]) so

$$\mathbf{F}(\mathbf{r}) \propto -\mathbf{e}_r \quad \text{for } r \gg r_0, \tag{14}$$

where $\mathbf{e}_r$ is the radial versor. Furthermore, we want the repulsive term to be divergent for $r \to 0$ to avoid body overlapping; for simplicity and relevance to classical physics we set

$$D(\mathbf{r}) \sim \frac{1}{r} \quad \text{for } r \ll r_0. \tag{15}$$

A simple form satisfying Eqs. (14) and (15) is

$$R(r) = \frac{r}{r_0} + \frac{r_0}{r}. \tag{16}$$

3. Full discomfort function

Assuming independence between θ and r (Appendix B), a simple form for D satisfying Eq. (14) $\forall\theta$ is

$$D^{\eta}_{ij}(r,\theta) = C_r R(r) + C_\theta \Theta^{\eta}(\theta). \tag{17}$$

The subscript ij recalls us that the definition of θ depends on the orientation of $\mathbf{r}_{ij}$ (Fig. 1) and that the discomfort of the two pedestrians is described by two different potentials if $\eta \neq 0$.

E. Interaction force

From Eqs. (11) and (17), and assuming $\theta > 0$, we may derive the force felt by a pedestrian i with relative position $\mathbf{r}_{ij}$ with respect to a socially interacting partner j in an *environment frame* whose y axis is aligned with $\hat{\mathbf{g}}$, as

$$F^{\eta}_x = \frac{C_r}{r_0}\left(\frac{r_0^2}{r^2} - 1\right)\sin\theta - \frac{4}{r}C_\theta(\theta - \theta_+)\cos\theta, \tag{18}$$

$$F^{\eta}_y = \frac{C_r}{r_0}\left(\frac{r_0^2}{r^2} - 1\right)\cos\theta + \frac{4}{r}C_\theta(\theta - \theta_+)\sin\theta, \tag{19}$$

where θ_+ is the angle in which Θ^{η} assumes the minimum

$$\theta_+ = (1-\eta)\frac{\pi}{2}. \tag{20}$$

In the $\theta \leqslant 0$ case we have to replace θ_+ with

$$\theta_- = -(1-\eta)\frac{\pi}{2}. \tag{21}$$

F. Center of mass and relative acceleration

Let us define

$$\varphi \equiv \theta_+ - \frac{\pi}{2} = -\eta\frac{\pi}{2} = -\left(\theta_- + \frac{\pi}{2}\right). \tag{22}$$

By substitution in Eqs. (18) and (19), we find that the acceleration $\dot{\mathbf{V}} \equiv (\mathbf{F}^{\eta}_{ij} + \mathbf{F}^{\eta}_{ji})/2$ of the center of mass with respect to environment frame, due to non-Newtonian internal force terms, results in

$$\dot{V}_x = \frac{4}{r}C_\theta\varphi\cos\theta, \tag{23}$$

$$\dot{V}_y = -\frac{4}{r}C_\theta\varphi\sin\theta, \tag{24}$$

where $0 < \theta \leqslant \pi$ is the angle giving the position of the pedestrian on the right (i.e., with $x \geqslant 0$) in the comoving frame with origin in $\mathbf{X}$ and y axis aligned to $\hat{\mathbf{g}}$. The presence of an $\eta \neq 0$ term causes thus an acceleration for the pedestrian group center of mass with magnitude $|a^{\eta}(r)|$, where

$$a^{\eta}(r) = \frac{4}{r}C_\theta\varphi. \tag{25}$$

The sign of $\dot{V}_y$ is always opposite to the sign of φ, so for $\eta > 0$ the non-Newtonian term accelerates the pedestrian group in the direction of the goal, while for $\eta < 0$ it decelerates it.

The relative acceleration is given by $\dot{\mathbf{v}} \equiv \mathbf{F}^{\eta}_{ij} - \mathbf{F}^{\eta}_{ji}$ and results in

$$\dot{v}_x = \frac{2C_r}{r_0}\left(\frac{r_0^2}{r^2} - 1\right)\sin\theta - \frac{8}{r}C_\theta\left(\theta - \frac{\pi}{2}\right)\cos\theta, \tag{26}$$

$$\dot{v}_y = \frac{2C_r}{r_0}\left(\frac{r_0^2}{r^2} - 1\right)\cos\theta + \frac{8}{r}C_\theta\left(\theta - \frac{\pi}{2}\right)\sin\theta, \tag{27}$$

Equations (26) and (27) are η independent and satisfy $\mathbf{f} \equiv \mathbf{F}^{\eta}_{ij} - \mathbf{F}^{\eta}_{ji} = 2\mathbf{F}^{0}_{ij}$, where $\mathbf{F}^0$ is the force obtained by derivation of the potential $D^0(\mathbf{r})$. This potential is invariant under inversion and thus satisfies $D^0_{ij} = D^0_{ji}$. We thus obtain that, as required in Sec. II B, the *relative dynamics* of the system is described by a single potential,

$$U(\mathbf{r}_i - \mathbf{r}_j) \equiv D^0(\mathbf{r}_i - \mathbf{r}_j). \tag{28}$$

The relative dynamics is thus described by Eqs. (7), (26), and (27), it is decoupled from the center-of-mass dynamics, and its statistical properties are given by the potential U.

[13] This repulsive term describes intergroup collision avoidance; in Ref. [26] we show that effective description of pedestrian avoidance needs to take into account relative velocity, but as long as the system is close to equilibrium $v \ll V$, and from the statistical point of view of Eq. (A2) a dependence only on $\mathbf{r}$ is sufficient for intergroup dynamics.

[14] Most probably pedestrians located at very large distances are not socially interacting, and their interaction force is weaker (a similar argument can be made for strongly nonabreast configurations). Nevertheless, in this work we develop the discomfort potential, assuming that pedestrians are always socially interacting, and extend it to any r and θ value. As a result, our method underestimates the probability of finding pedestrians very far from equilibrium, even when it describes very well the behavior around equilibrium (see, for example, Fig. 5).

The dynamics of the center of mass, on the contrary, depends on the relative dynamics. Since the potential U is symmetrical under $\theta \to \pi - \theta$, we see from Eq. (23) that at statistical equilibrium $\overline{V}_x = 0$.[15] Regarding V_y, for a "low-temperature" system, we may assume the relative system to be close to the minimum of U, i.e., to have $\mathbf{r} \approx (r_0, \pm\pi/2)$. For such a configuration, the acceleration given by Eq. (25) is directed along y (i.e., along the goal direction $\hat{\mathbf{g}}$), causing a higher preferred velocity for $\eta > 0$ and a lower one for $\eta < 0$. The total acceleration for the two-pedestrian group center of mass will be given by the sum of the terms of Eqs. (2) and (25). Since v_p is by definition equal to the velocity of pedestrians outside groups $v^{(1)}$, the velocity of pedestrians in groups of two is (at least for a zero-temperature equilibrium configuration)

$$v^{(2)} = v^{(1)} - a^{\eta}(r_0)\tau. \tag{29}$$

As we show in Table I, empirical data suggest $v^{(1)} > v^{(2)}$ and thus $\eta < 0$. In Appendix C we show how to improve the estimate of Eq. (29) by taking thermal effects into account.

G. Model parameters

The parameters C_r and C_θ have the dimension of the square of a velocity. For $r \gg r_0$ we have

$$\mathbf{F}(\mathbf{r}) = -\frac{C_r}{r_0}\mathbf{e}_r. \tag{30}$$

From this equation we may get the order of magnitude of C_r. We may expect the value for the acceleration towards the partner when at a large distance to be roughly equivalent to the maximum acceleration towards the goal.[16] Using Eq. (2), the value of τ reported in Ref. [26] and the velocity of single pedestrians in Table I, we have a maximum acceleration $\approx a^{\max} = 2\mathrm{m/s}^2$, so we may guess

$$C_r = r_0\, a^{\max}. \tag{31}$$

The data regarding the statistical behavior of two-pedestrian groups are not sufficient to calibrate all the values of the model parameters,[17] unless we use Eq. (31), as we do in Sec. IV. On the opposite, in Sec. VI E we calibrate all parameters based on the two- and three-person group data, without relying on Eq. (31).

We may estimate the contribution of the radial and angular part of U by computing its (adimensional) second derivatives in the minimum

$$\left.\frac{\partial^2 U}{\partial^2 \theta}\right|_{\theta=\pm\frac{\pi}{2}} = 4C_\theta; \quad \left.\frac{\partial^2 U}{\partial^2\left(\frac{r}{r_0}\right)}\right|_{r=r_0} = 2C_r. \tag{32}$$

The two terms are equivalent for

$$\tilde{C}_\theta = \frac{C_r}{2}. \tag{33}$$

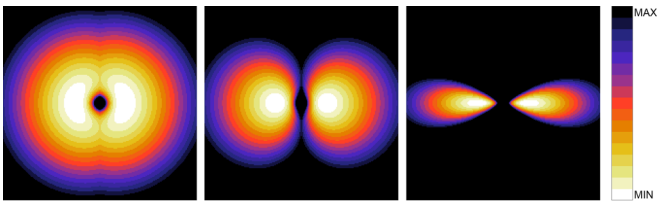

FIG. 2. (Color online) Two-dimensional dependence of the discomfort potential U for different values of the ratio C_r/C_θ in a square area of size $4r_0$ (high values in black and low values in white). From left to right, $C_\theta = \tilde{C}_\theta/5$, $C_\theta = \tilde{C}_\theta$, and $C_\theta = 5\tilde{C}_\theta$ [see Eq. (33)].

Figure 2 shows the qualitative behavior of the potential U for values $C_\theta = \tilde{C}_\theta/5$, $C_\theta = \tilde{C}_\theta$, and $C_\theta = 5\tilde{C}_\theta$.

III. EMPIRICAL OBSERVATIONS

A. Data collection

We tracked pedestrian motion in two different areas of a pedestrian underground facility in Umeda, Osaka (Japan), for 6 h in each area. The pedestrian areas consisted of a few corridors connecting a railway station to a shopping mall, each area being around 500 m^2. The environments are described in detail in Ref. [44], and the pedestrian tracking data are available at Ref. [45]. The average pedestrian density in the environment resulted in $\approx$0.03 pedestrians per square meter while the width of the corridors varied between 4 and 7 m, meaning that the average distance from a pedestrian to another pedestrian outside their group, or to a wall, is expected to be larger than the spatial size of the group.[18] We thus assume that collision avoidance is not a dominant behavior in this environment.

The pedestrian positions were determined at time intervals of $\approx$50 ms using a laser range-finder tracking system that has a precision of $\approx$50 mm [46]. We smoothed the tracked positions on time windows of 500 ms to further improve the precision and to reduce the effect of gait in position measurement.[19] Pedestrian velocity is computed as the ratio of the displacement vector between two (smoothed) consecutive tracking positions and the time window.

We also video recorded each experimental area using two different "frontal view" cameras (Fig. 3) to observe the social

[15] This can be verified explicitly by replacing $\sin\theta$ with $\cos\theta$ in Eq. (C1).

[16] By maximum acceleration we mean the acceleration felt by a single pedestrian with $\mathbf{v} = 0$ in the environment frame.

[17] Since the observable effects are determined by the three equations (26), (27), and (29).

[18] We may introduce the following "rule of thumb" to define the range of density up to which the group structure may be considered as not perturbed by collision avoiding beyond the conditions of Eq. (4): assuming $r_0 \approx 0.75$ m to be the average distance between two interacting pedestrians, we ask the size of the environment to be larger than nr_0, and the density smaller than $(nr_0)^{-2}$, in order to consider an n pedestrian group to be "free walking" in the meaning of Eq. (4). It is nevertheless very difficult to state in a rigorous way what is the value of pedestrian densities at which the approximations leading to Eq. (4) are valid, and thus it will be important in future to compare the results of this paper with the behavior of pedestrian groups in natural environments at even lower densities, when such data will be available.

[19] The time length of a pedestrian stride is roughly 0.5 s [47].

FIG. 3. (Color online) Camera view of the experimental area.

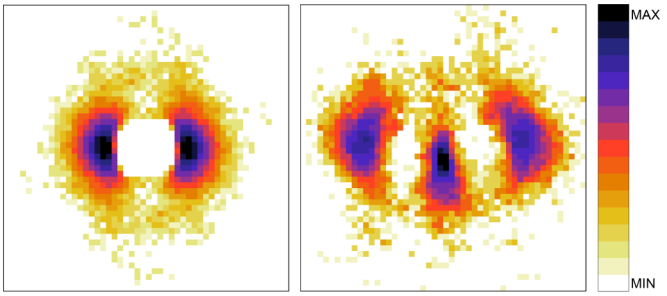

FIG. 4. (Color online) Empirical *pdf*s in the center-of-mass frame, for two- (a) and three- (b) pedestrian groups. High-probability cells in black and low-probability cells in white. The same data are shown in Figs. 5 and 10 along with a quantitative color bar.

interaction between the pedestrians for a sufficiently long time (pedestrians are usually tracked and observed for tens of seconds). This front-view camera-based observation of social interaction was possible because the cameras are not needed for tracking and the density was relatively low (otherwise top-view cameras would have been necessary).

Two *coders* (nontechnical staff members of our laboratory) were asked to identify all the social groups in the environment and their members. In order to do that, they were asked to use all the information available from the videos, such as relative position, coherent motion, and social clues, including conversation, gaze exchange, and age, sex, and clothing. Furthermore, the coders were asked to annotate the groups, and the individuals in each group, for which they could identify explicit social interaction clues (namely conversation, or explicit gaze exchange). For an evaluation of the agreement between coders, see Appendix D.

B. Results

We are interested in *fully connected socially interacting groups*, i.e., groups in which, from the point of view of social interaction, no disconnected subgroup was present. For the scope of this paper we use groups of size $n = 2, n = 3$, and $n = 4$, and we use only social groups for which *both* coders agreed on the size of the group and on all the members of the group being involved in social interaction. In this way, we should be able to avoid *false positives*, i.e., groups that were coded as interacting but actually were not.[20] In contrast, we could have some *false negatives*, but this is not a problem provided that the number of fully interacting groups coded by both coders is high enough for a significant statistical analysis. Table I reports the number of fully interacting groups for each size, along with the number of trajectory points, and the average, standard deviation and standard error of their velocity distributions.[21]

We are interested in the behavior of interacting and walking pedestrians, and for this reason we do not consider data points in which one of the members of the group has a velocity slower than 0.5 m/s.[22] For each group we ideally would like to compute the positions in the reference frame comoving with the center of mass and with the y axis aligned to the goal. However, since the goal information is not available, we assume that the group velocity is aligned to the goal direction,

$$\mathbf{V}/V \approx \hat{\mathbf{g}}, \tag{34}$$

which is reasonable unless the system is very far from equilibrium. Finally, we measure the empirical probability distribution for pedestrians in the group center-of-mass frame, by dividing the space in regular cells of linear dimension 0.05 m and averaging occupancy over all groups and times. Figure 4 shows a logarithmic plot of the pedestrian distribution for two-pedestrian and three-pedestrian groups, in square areas of linear size 2.5 m centered around the center of mass. We can see a qualitative agreement between the shape of the isopotential curves of Fig. 2(a) (low C_θ value) and the isoprobability curves of Fig. 4(a), with the potential minima corresponding to the probability maxima. These probability distributions are qualitatively similar to those of Ref. [4], suggesting a cross-cultural value.

IV. MODEL CALIBRATION

A. Boltzmann distribution calibration

According to the ergodic principle,[23] and following the results of Eqs. (7), (26), and (27), the probability[24] of finding

[20]Pedestrians were labeled as interacting or not interacting, without labeling the time at which the interaction happened. Interacting groups may have been noninteracting for some time, with effects on empirical distributions, in particular regarding the tails.

[21]These values are obtained computing, first, the average velocity for each group and then computing the mean, standard deviation, and error on the average velocity distributions. If we just compute averages and standard deviations on the overall velocity distribution of all pedestrians at all times, slower groups have a larger impact by being longer in the tracking area, and the corresponding results are 1310 ± 240 mm/s for $n = 1$, 1137 ± 209 for $n = 2$, 1099 ± 192 for $n = 3$, and 1059 ± 187 for $n = 4$.

[22]We chose this threshold considering the velocity distributions (see Table I). The validity of the threshold is given by the fact that, after removing the velocities under the threshold, we obtain a normal distribution whose average is a few standard deviations higher than the threshold itself. For a detailed discussion, see Ref. [44].

[23]Provided that the sum and the integrals of Eq. (A2) are performed over large-enough values of N and T_k.

[24]In this work, when dealing with 2D probability distributions, we divide the 2D space in uniform cells and normalize ρ according to

TABLE II. Model parameters obtained calibrating only on two-pedestrian data [Eq. (37)] and on two- and three-pedestrian data [Eq. (47)]. r_0 in m, C_r and C_θ in m^2/s^2, σ in m/s^2, φ in degrees.

	r_0	C_r	C_θ	η	σ
Eq. (37)	0.752	1.5	0.16	-0.23 ($\varphi = 20$)	1.09
Eq. (47)	0.745	0.62	0.08	-0.43 ($\varphi = 39$)	0.77

the pedestrian in a cell of sufficiently small area centered in $\mathbf{r}^{\text{c.m.}} = (x_i, y_j)$ is given, for a two-pedestrian group, by

$$\rho_B(x_i, y_j) = \frac{e^{-\frac{U(2x_i, 2y_j)}{T_\Xi}}}{\sum_{k,l \in \text{cells}} e^{-\frac{U(2x_k, 2y_l)}{T_\Xi}}}, \tag{35}$$

where the "temperature" T_Ξ is determined by the equilibrium between the $-\mathbf{v}/\tau$ and $\boldsymbol{\Xi}$ terms in Eq. (7).[25]

While keeping $C_r/r_0 = 2\ m/s^2$ [Eq. (31)], we may calibrate r_0, C_r/C_θ, and T_Ξ in order to minimize the difference between the probability distribution given by the model through Eq. (35), ρ_B, and the one empirically observed, ρ_E. We thus searched, using a genetic algorithm, for the values of the parameters that minimize

$$\varepsilon_B = \sum_{i,j \in \text{cells}} \frac{(\rho_B(x_i, y_j) - \rho_E(x_i, y_j))^2}{\rho_E(x_i, y_j)}, \tag{36}$$

i.e., the relative error weighted by the number of observations per cell.[26]

B. Parameters value

The optimal values resulted to be $r_0 = 0.752$ m, $C_\theta = 0.157\ m^2/s^2$ [$\approx \tilde{C}_\theta/5$, refer to Eq. (33)] and $T_\Xi = 0.053\ m^2/s^2$ (see also Table II for parameter values). As already suggested by the qualitative similarity between Figs. 2(a) and 4(a), the contribution of the angular term to the discomfort seems to be smaller than the radial one.

Figure 5 compares the logarithmic 2D plots for the observed [Fig. 5(a)] and modeled [Fig. 5(b)] probability distributions. The model has a tendency to underestimate the probabilities far from equilibrium[27] but describes properly the 2D distribution around the maxima. Figure 6(a) shows the y dependence of ρ_E and ρ_B for different values of x, while Fig. 6(b) shows the x dependence of ρ_E and ρ_B for different values of y.

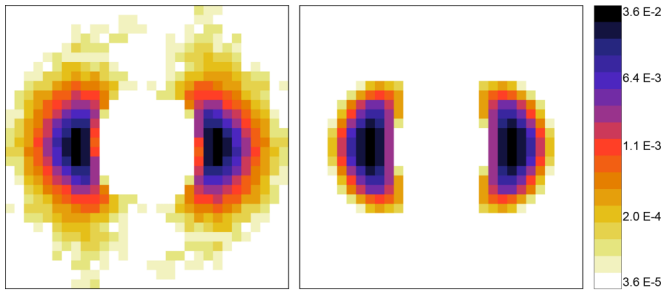

FIG. 5. (Color online) (a) Empirical *pdf* ρ_E in a square area of linear size 1.5 m centered on the center of mass. (b) ρ_B in the same area. The graph shows the probability of observing a pedestrian in each cell, according to the logarithmic color bar. Probabilities below $\rho^{\min} = 3.6 \times 10^{-5}$ are fixed to $\rho^{\min}$.

C. Estimate of η

Using Eqs. (25) and (29), and Table I to know the difference between the velocity of an independent pedestrian, $v^{(1)}$, and a pedestrian in a group of 2, $v^{(2)}$, and the value $\tau = 0.66$ s from Ref. [26], we get $\varphi \approx 0.32$ rad (18.5°) or $\eta \approx -0.2$. This value assumes that the pedestrians are always at the equilibrium position, which is only an approximation for $\boldsymbol{\Xi} \neq 0$. In the next section, we rely on numerical integration to obtain the value of φ for a system with noise (i.e., with nonzero temperature). See also the discussion in Appendix C for an analytical estimate of the thermal effects on pedestrian velocity.

V. NUMERICAL INTEGRATION

For practical applications we need a numerical integrator of Eq. (4) [i.e., a simulator of the pedestrian group behavior; in this work the terms *numerical integration* of Eq. (4) and *simulation* of the pedestrian system are to be considered equivalent]. In order to do that we need an estimate of the noise term $\boldsymbol{\Xi}$, and we need to check that, using this appropriate noise value, the statistical behavior of the system is equivalent to the empirical one and to the theoretical result of Eq. (35).

In this section we use a first-order Euler integrator (see Appendix E) with time step $\Delta t = 0.1$ s[28] and assume that Ξ_x

$\sum_{i \in \text{cells}} \rho_i = 1$, and thus ρ is dimensionally a probability. The same convention is used when we show 1D "slices" of the 2D distributions, as in Figs. 6 and 12. On the contrary, when showing actual 1D probability distribution functions, as in Figs. 7, 11, and 13, we use the normalization condition $\int \rho(z) dz = 1$.

[25]Equation (35) may be obtained by writing $\rho_B(\mathbf{r}_i, \mathbf{r}_j) = C \exp(-U(\mathbf{r}_i - \mathbf{r}_j)/T_\Xi)\ \delta(\mathbf{r}_i - \mathbf{r}_j)$, integrating over $\mathbf{r}_j$, and considering that the overall probability distribution is the normalized sum of the two identical i and j distributions.

[26]Since ρ is a probability, ε_B is a pure number. The error function is obtained by computing, for each cell, the square of the ratio of the difference between empirical and modeled probabilities over the empirical probability, $\Delta\rho^2/\rho_E^2$, and then multiplying it by the probability of observing the system in such a cell, ρ_E. The denominator is thus ρ_E and high-probability points (maxima) are given a higher weight with respect to a straightforward relative error computation.

[27]The description is good up to a few standard deviations, so differences are visible only in log scale.

[28]This is a rough integrator from the computational physics point of view, but it is standard in pedestrian crowd simulations, so it is important to verify that such an integrator may reproduce the analytical results. It is also arguable that a first-order integration with a time step of order Δt is a more realistic way to realize the pedestrians' decision process than a refined integrator (as, for example, a Runge-Kutta 4) with a shorter step, even if the latter provides results closer to the continuous ones.

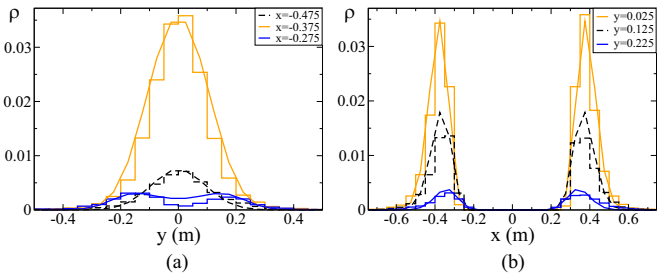

FIG. 6. (Color online) (a) y dependence of ρ_E compared to the y dependence of ρ_B for different values of x. (b) x dependence of ρ_E compared to the x dependence of ρ_B for different values of y. To facilitate the distinction, in both figures, ρ_B is shown as a continuous function rather than a histogram.

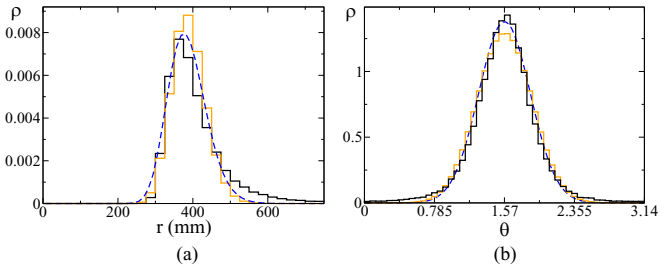

FIG. 7. (Color online) (a) Comparison between $r^{\text{c.m.}}$ distributions in a two-pedestrian group. Solid black: Empirical distribution. Solid orange (light gray): Numerically integrated system. Dashed blue (dark gray): analytical result of Eq. (35) (shown as a continuous function). (b) Same comparison for θ.

and Ξ_y are given by two identical normal distributions with standard deviation σ. Keeping the values of parameters C_r, C_θ, and r_0 fixed as calibrated in the previous section, we use a bisection method on the error function

$$\varepsilon_S = \sum_{i,j\in\text{cells}} \frac{(\rho_S(x_i,y_j) - \rho_E(x_i,y_j))^2}{\rho_E(x_i,y_j)} \tag{37}$$

to find the value of σ that reproduces the empirical values.[29] Here ρ_S is the simulated probability distribution for the position of the pedestrian in the reference system comoving with $\mathbf{X}$ and with the y axis aligned to $\mathbf{V}$,[30] integrated numerically over a time interval T long enough in order not to have a T dependence in the results.[31]

We find that the similarity between ρ_S and ρ_E is maximized by adding a white-noise therm with $\sigma \approx 1.09$ m/s^2 to each step of the numerical integration.[32] We are going to use this value of σ in the following numerical integrations of the system.

The average velocity of the numerically integrated two-pedestrian group resulted in 1.178 m/s, as predicted slightly higher than the analytical result (29) (which is valid for a noiseless system). We used a bisection optimization to find the value of η that gives a velocity of 1.160 ± 0.146 m/s; the result is $\eta = -0.23$ ($\varphi = 0.36$ radians or $\approx 20.5^\circ$). We discuss the effects of noise on group velocity in Appendix C.

To verify that the results of our numerical integrator are basically equivalent to those of the previous section, and thus a good approximation of the empirical ones, Fig. 7 shows a comparison among the empirical, analytical, and simulated r and θ probability distributions.

VI. THREE PEOPLE

A. First-neighbor interaction

According to Ref. [5], unconstrained n pedestrian groups walk in an abreast configuration, keeping a distance between each first neighbor, almost equivalently to the two-pedestrian group distance. References [4,13,14] suggest bent formations for such groups, and Ref. [14] suggests that large groups are not stable. Still, even the presence of metastable structures with pedestrians located at distances of $\approx(n-1)r_0$ is not in agreement with a straightforward application of Eq. (1) with interaction forces given by Eqs. (18) and (19) and j running over all $j \neq i$. Even for the three pedestrian groups that we observed, as shown in Table III, the central angle in the V formation is close to π, and the distance between the pedestrians on the wings is just slightly smaller than $2r_0$,

TABLE III. Average values and standard deviations of the main observables obtained using parameters calibrated on two- and three-pedestrian data [Eq. (47)] compared to those obtained using only two-pedestrian data [Eq. (37)] and to empirical data. r and θ without any index stand for the two-pedestrian distributions. For empirical distributions, the mode is shown in place of $\overline{\theta}$ and $\overline{r}$. r variables in meters, θ variables in radians, v ones in meters per second. For angular variables we use linear statistics on $-\pi < \theta \leqslant 0$.

	Eq. (37)	Eq. (47)	Empirical
r	0.78 ± 0.09	0.77 ± 0.1	0.82 ± 0.19
θ	−1.57 ± 0.31	−1.57 ± 0.29	−1.57 ± 0.35
$\overline{r}$	0.76	0.78	0.73
$\overline{\theta}$	1.46	1.38	1.42
r_{12}	0.79 ± 0.09	0.81 ± 0.1	0.85 ± 0.22
θ_{12}	−1.46 ± 0.3	−1.38 ± 0.28	−1.29 ± 0.54
r_{13}	1.54 ± 0.13	1.57 ± 0.14	1.46 ± 0.3
θ_{13}	−1.57 ± 0.23	−1.57 ± 0.25	−1.59 ± 0.32
$v^{(2)}$	1.160 ± 0.15	1.160 ± 0.1	1.159 ± 0.17
$v^{(3)}$	1.098 ± 0.12	1.110 ± 0.09	1.112 ± 0.14

[29] The calibration of all parameters could have been performed using a multidimensional optimization algorithm on Eq. (37), as we do for Eq. (47) in Sec. VI. Nevertheless, calibration on (35) does not rely on numerical integration and is thus less computationally expensive.

[30] In this way, the computation of the simulation density distribution, ρ_S, is completely equivalent to the experimental one of ρ_E, while for ρ_B we used the reference frame aligned with $\mathbf{v}_p$.

[31] This is basically a numerical realization of Eq. (A1). We verified that the results were equivalent for $T = 10^5$ and $T = 10^6$ s and used the latter value in all the following results.

[32] Since we did not deal with the problem of numerically implementing Eq. (4) for different Δt time steps, the validity of the proposed σ values has been tested only for the proposed Euler method and $\Delta t = 0.1$ s.

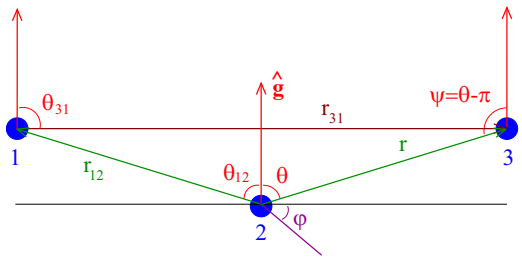

FIG. 8. (Color online) Variable definitions for three pedestrian groups.

suggesting that the forces of Eqs. (18) and (19) do not act among them.[33]

Nevertheless, we may show that the proposed potential can describe the three-person behavior in good agreement with the empirical observations, provided that it is used as a first-neighbor interaction term. Let us assume that this term is the leading one in determining the group configurations and examine its consequences for a three-person group. Let us number the pedestrians in Fig. 8 as 1, 2, and 3 from left to right in a reference frame with the y axis aligned to $\hat{\mathbf{g}}$, i.e., with $x_1 \leqslant x_2 \leqslant x_3$. The dynamics of the system is determined by Eq. (4) in which, for each i, the values assumed by j are $i \pm 1$.

B. Equilibrium configuration: V formation

To compute the equilibrium configuration of a noiseless system we may use a frame centered on the position of pedestrian 2 and with y axis aligned with $\hat{\mathbf{g}}$. Since the discomfort function determining the interaction of 2 with the pedestrians on the wings, $D_{2j}(\mathbf{r}_{2j})$, is symmetrical under the operation $\theta \to -\theta$, we seek a configuration that is symmetrical under reflection on the y axis (Fig. 8). In such a frame, and for such a symmetrical configuration, the position of pedestrian 1 is given in polar coordinates by $\mathbf{r}_{12} = (r_{12},\theta_{12}) = (r, -\theta)$ and, by symmetry, the position of 3 by $\mathbf{r}_{32} = (r_{32},\theta_{32}) = (r,\theta)$, with $0 < \theta < \pi$. The coordinates of the center of mass in this frame are $X = 0$, $Y = 2r/3\,\cos\theta$, and if we find in it a configuration in which all pedestrians have the same acceleration with respect to the environment, such a configuration represents a relative dynamics equilibrium. By explicit computation of the forces, or by symmetry principles, we may verify that for each configuration as in Fig. 8 we have

$$F_{21}^y = F_{23}^y; \quad F_{12}^y = F_{32}^y; \quad F_{21}^x = -F_{23}^x; \quad F_{12}^x = -F_{32}^x. \tag{38}$$

As a consequence, to have an equilibrium configuration, we require, for the x component,

$$F_{32}^x = F_{12}^x = F_{21}^x + F_{23}^x \;\Rightarrow F_{32}^x = 0 \tag{39}$$

and, for the y component,

$$F_{32}^y = F_{12}^y = F_{21}^y + F_{23}^y \;\Rightarrow F_{32}^y = 2F_{23}^y. \tag{40}$$

We write these expressions explicitly as functions of r and θ using Eqs. (18) and (19) and call $\overline{\theta}$ and $\overline{r}$ the values for which Eqs. (39) and (40) are satisfied. If such values exist, the system has an equilibrium configuration symmetrical around $\hat{\mathbf{g}}$, corresponding to a Λ formation (central pedestrian on the front) for $\overline{\theta} > \pi/2$, an abreast one for $\overline{\theta} = \pi/2$, and a V formation (central pedestrian on the rear) for $\overline{\theta} < \pi/2$.

After some algebra, we find that $\overline{\theta}$ is determined only by φ [i.e., by η, Eq. (22)],

$$3\left(\overline{\theta} - \frac{\pi}{2}\right) + \varphi(1 - 4\cos^2\overline{\theta}) = 0, \tag{41}$$

while $\overline{r}$ is a function of r_0, C_r/C_θ, and η,

$$\frac{r_0}{\overline{r}} - \frac{\overline{r}}{r_0} = \frac{4C_\theta\cos\overline{\theta}}{C_r\sin\overline{\theta}}\left(\overline{\theta} - \frac{\pi}{2} - \varphi\right). \tag{42}$$

In Fig. 9(a) we show the numerical solution of Eq. (41), $\overline{\theta}(\eta)$, while in Fig. 9(b) we show the numerical solution of Eq. (42), $\overline{r}(\eta,r_0,C_r/C_\theta)$.

Recalling Eq. (29) and Table I, since $v^{(1)} > v^{(2)}$ we have $\eta < 0$ and thus $\overline{\theta} < \pi/2$. Our model thus predicts that for a noiseless three-pedestrian system, i.e., a system described

[33] We performed the same analysis of Sec. VI B, i.e., the search of a V-formation equilibrium configuration, assuming interaction between all pedestrians. The numerical analysis gives a value of $\overline{r} = 0.61$ m for the distance between first neighbors, $\overline{\theta} = 1.3$ rad for the half central angle of the V formation, and a velocity for a noiseless three-person group of 0.85 m/s. These are not completely unrealistic numbers, and such a "fully interacting" three-person group could actually exist, but such evidence is not present in our observations.

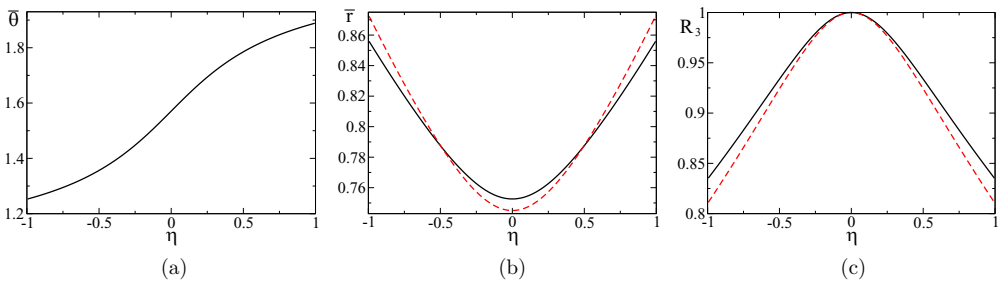

FIG. 9. (Color online) (a) $\overline{\theta}(\eta)$. (b) $\overline{r}(\eta)$ for calibrated r_0, C_r, and C_θ values. (c) $R_3(\eta)$. In the latter two figures, black solid lines use parameters calibrated on two-pedestrian data [Eq. (37)], while red dashed lines use parameters calibrated on two- and three-pedestrian data [Eq. (47)].

by Eq. (4) with $\Xi = 0$, the equilibrium configuration is a V formation. For a system with noise, this turns into the most probable configuration or the stable configuration in the meaning of Ref. [14]. The V formation with the central pedestrian on the rear is thus a consequence of applying the first-neighbor version of our model to a three-pedestrian system.

Using the parameter values calibrated in Sec. V we find $\overline{\theta} \approx 1.46$ rad (83°) and $\overline{r} \approx 0.76$ m. Since the parameters of Sec. V depend on Eq. (31), that provides an estimate of the order of magnitude of the maximum acceleration Eq. (30), we expect $\overline{\theta}$ and $\overline{r}$ to provide the *correct order of magnitude of the deviation from abreast walking for three-person groups*. If the maximum acceleration Eq. (30) was explicitly measured, the predictive value of the model could be tested more strictly.

C. Three-person group velocity

We can now estimate the velocity of the three-person group. In an abreast formation, which is not an equilibrium one for $\eta \neq 0$, the pedestrian at the center feels a force opposed to $\mathbf{v}_p$ with intensity $8C_\theta\varphi/r_0$, i.e., twice the value given by Eq. (25) felt by the other two pedestrians. As a result, for the group velocity we obtain, from Eqs. (25) and (29),

$$v^{(3)} \approx v^{(1)} - \tfrac{4}{3}a^\eta(r_0)\tau = v^{(1)} - \tfrac{4}{3}\left(v^{(1)} - v^{(2)}\right). \quad (43)$$

According to Eq. (43) the difference between the velocity of an independent pedestrian and the velocity of a three-pedestrian group should be roughly 4/3 the difference between the velocity of an independent pedestrian and the velocity of a two-pedestrian group. Applying this equation to the values of Table I, we obtain an expected value of $v^{(3)} = 1100$ mm/s, i.e., less than one standard error from the observed value. This estimate can be improved taking into account that the equilibrium configuration is not abreast and that the actual y acceleration is

$$\begin{aligned} A_3 &= -F_{12}^y \\ &= -\frac{C_r}{r_0}\left(\frac{r_0^2}{\overline{r}^2} - 1\right)\cos\overline{\theta} - \frac{4C_\theta}{\overline{r}}\left(\overline{\theta} - \frac{\pi}{2} - \varphi\right)\sin\overline{\theta}. \end{aligned} \quad (44)$$

Let us define

$$R_3 = \frac{A_3}{\frac{4}{3}a^\eta(r_0)}, \quad (45)$$

of which Fig. 9(c) shows a numerical solution as a function of η for the calibrated parameters. Since R_3 attains a minimum value >0.8 for $|\eta| = 1$, Eq. (43) gives a good approximation of the three-pedestrian group velocity for any value of η [i.e., regardless of our assumption Eq. (31)[34]]. The value for the three-person group velocity is

$$v^{(3)} = v^{(1)} - \tfrac{4}{3}R_3\left(v^{(1)} - v^{(2)}\right), \quad (46)$$

[34] $\overline{r}$ and R_3 depend only on the ratio C_r/C_θ and not on the individual values of these parameters, and thus the curves of Fig. 9 do not depend on the estimate of Eq. (31).

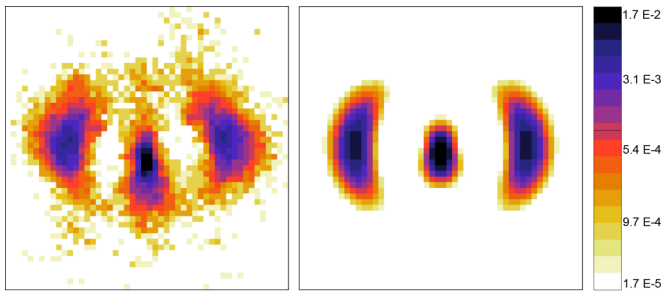

FIG. 10. (Color online) (a) Empirical *pdf* $\rho_E^{(3)}$ in a square area of linear size 2.5 m around the center-of-mass reference frame for a three-person group. (b) $\rho_S^{(3)}$ in the same area. The graph shows the probability of observing a pedestrian in each cell, according to the logarithmic color bar. Probabilities outside $[1.7 \times 10^{-5}, 1.7 \times 10^{-2}]$ are fixed to the extreme values. For the simulation, we used model parameters calibrated only on the two-person distribution [Eq. (37)].

which for the parameter values calibrated in Sec. V yields $v^{(3)} = 1.104$ m/s ($R_3 = 0.98$).[35]

D. Simulation

Figure 10 compares the empirical three-pedestrian position distribution to the one predicted by numerical integration of our model using first-neighbor interaction in Eq. (4) with the parameters calibrated in Secs. IV–V.[36] The simulation provides a qualitative description of the three-pedestrian 2D probability distribution, describing correctly the structure of the stable configuration (maxima position) and to a good extent also the shape of the distribution around these maxima. Similarly to the two-pedestrian group case, the model underestimates the probability of being located far from equilibrium, this deviation being more severe in the three-pedestrian case.

From a quantitative point of view, for the simulated system we have $\langle\theta_{12}\rangle = 1.46$ rad (see Table III for a recap of average values and standard deviations of empirical and modeled observables), $\langle r_{12}\rangle = 0.79$ m and $v^{(3)} = 1.098$ m/s, in agreement with Eq. (46) and Table I. For the empirical distributions we have $\langle r_{12}\rangle = 0.85$ m and $\langle\theta_{12}\rangle = -1.29$ rad, showing that *the order of magnitude* of deviation from abreast walking is correctly predicted.

The prediction is also qualitatively quite accurate if we focus on the position of the maximum value of the r_{12} and θ_{12} distributions (Fig. 11). The difference between the average values as described by the model with respect to the

[35] Equation (46) was derived for a noiseless system, but our simulations show that it applies also to the numerically simulated noisy systems, provided that by $v^{(2)}$ we mean the actual average velocity and not the lower analytical value given by Eq. (29). See the discussion in Appendix C about the effect of noise (nonzero temperature) on group velocity.

[36] In simulations, if two pedestrians switch position, their labels are changed. In other terms, the central pedestrian is the one that is at the central position at a given time and not the one that started at the center.

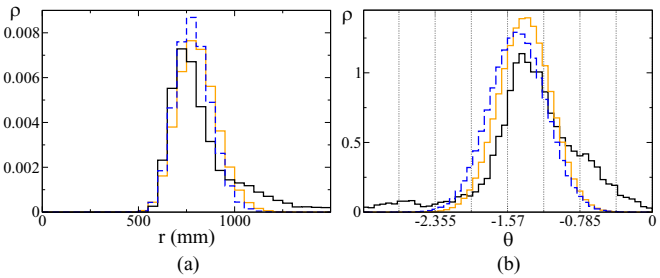

FIG. 11. (Color online) (a) *pdf* for the distance between the pedestrian on the left and the central one, r_{12}. Empirical distribution in solid black; simulation using parameters calibrated only on two-pedestrian group data [Eq. (37)] in dashed blue (dark gray); simulation using parameters calibrated on two- and three-pedestrian groups [Eq. (47)] in solid orange (light gray). (b) Same comparison for the angle between the pedestrian on the left and the central one, θ_{12}.

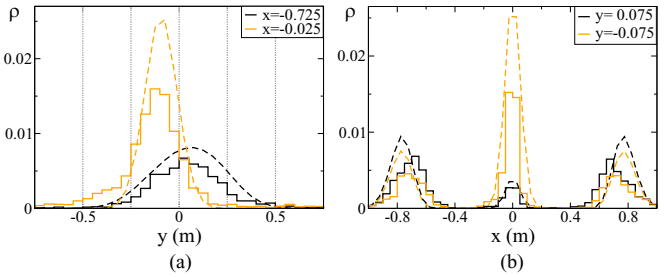

FIG. 12. (Color online) (a) y dependence of $\rho_E^{(3)}$ (solid line) compared to the y dependence of $\rho_S^{(3)}$ (dashed) for different values of x. The black lines show the y dependence along the most probable x position of the pedestrian on the left wing, while orange (light gray) lines are used along the x position of the central pedestrian. (b) x dependence of $\rho_E^{(3)}$ (solid line) compared to the x dependence of $\rho_S^{(3)}$ (dashed) for different values of y. The orange (light gray) lines show the x dependence along the most probable y position of the central pedestrian, while the black lines are used along the y position of the wing pedestrians. In both figures $\rho_S^{(3)}$ was obtained using parameters optimized using Eq. (47), i.e., both two- and three-pedestrian group data.

empirical ones is mainly due to the fact that the model fails in describing the fat tail for $r_{12} \gg r_0$ and the asymmetry of the θ_{12} distribution.

E. Calibration on two- and three-pedestrian data

In order to avoid using Eq. (31) to estimate the maximum acceleration Eq. (30), we may calibrate all the model parameters using both two- and three-pedestrian distribution data. While this approach does not have the predictive value of the one we followed up to now (using only two-pedestrian data to qualitatively and quantitatively predict the stable configuration and group velocity of three-pedestrian groups), it allows us to obtain the best possible estimate for the parameters and to investigate the extent to which the model can describe both two- and three-person group behavior.

We use a genetic algorithm to find the parameter values that minimize Eq. (37) for both two- and three-pedestrian distributions and that provide the correct two- and three-pedestrian group velocity. Namely, the error function minimized by the algorithm is

$$\varepsilon_{S'} = \sum_{k,i,j} \frac{\left(\rho_S^{(k)}(x_i,y_j) - \rho_E^{(k)}(x_i,y_j)\right)^2}{\rho_E^{(k)}(x_i,y_j)} + \frac{\left(v_S^{(k)} - v_E^{(k)}\right)^2}{\left(\sigma_e^{(k)} + \sigma_e^{(1)}\right)^2}, \tag{47}$$

with $k = 2,3$, where $\rho_S^{(k)}$ is the k-person-simulated distribution, $\rho_E^{(k)}$ is the corresponding empirical one, $v_S^{(k)}$ is the average k-person group velocity according to simulations, while $v_E^{(k)}$ and $\sigma_e^{(k)}$ are the empirical k-person group average velocity and standard error as reported in Table I.[37]

Table II shows the calibrated values, comparing them with those obtained using Eq. (37). The ratio C_r/C_θ was lower but close to the value obtained calibrating on two-pedestrian data, resulting in a two-pedestrian distribution basically equivalent to the one we found previously (see Table III). The ratio C_r/r_0 is now ≈ 1, so the maximum acceleration is ≈ 1 m/s^2, a factor 2 weaker than our estimate. As a result, to obtain the correct value for a^η [Eq. (25)], we have an increase in the absolute value of η.

Table III shows the average values and standard deviations of the main observables obtained using parameters calibrated on two- and three-pedestrian data [Eq. (47)], comparing them to those obtained using only two-pedestrian data [Eq. (37)] and to empirical data.

As evident from Table III and Fig. 11, the parameters calibrated using Eq. (47) provide a better quantitative description of the deviation from abreast walking, even though they still fail to describe the asymmetric nature of the θ_{12} distribution. In Fig. 12(a) we compare the y dependence of $\rho_E^{(3)}$ and $\rho_S^{(3)}$ [optimized according to Eq. (47)] for different values of x, while in Fig. 12(b) we perform the same comparison for the x dependence at different values of y.[38]

This comparison shows that the position of the maxima, both for the pedestrian on the center and for the pedestrians on the wings, is identified with a precision of at least 10 cm. In particular, the distribution around the equilibrium position for both the central and wing pedestrians is very well described, in maxima and deviations, along the y direction (direction of motion).[39] In the x direction, while the position of the central pedestrian is well identified, the pedestrians on the wings are

[37] In Eqs. (36) and (37), dividing by ρ instead of ρ^2, we took into account the different number of data points related to each ρ value, i.e., we gave a larger weight to high ρ values. In Eq. (47) we use the same principle, but since both $\rho^{(2)}$ and $\rho^{(3)}$ are normalized so that $\sum_{i\in\text{cells}} \rho_i^{(k)} = 1$, we are not taking into account in the ρ part of the error function the fact that the two-person observations are based on a larger amount of data (Table I), in order not to create an unbalance in calibration between the two-person and three-person distributions.

[38] These x and y values correspond to the ρ_S maxima.

[39] Due to the fat tails in empirical distributions, and thus to the wider spread of the 2D normalized distributions in the direction not shown, the empirical distributions appear to have a lower integral at fixed x or fixed y.

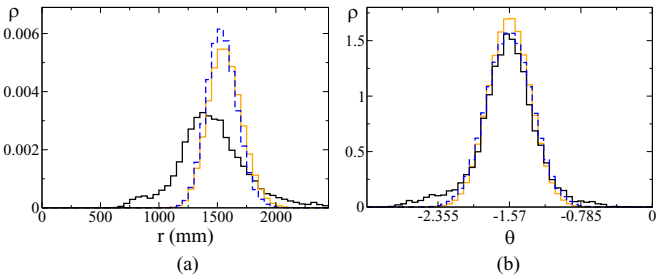

FIG. 13. (Color online) (a) *pdf* for the distance between the pedestrians on the wings, r_{13}. Empirical distribution in solid black; simulation using parameters calibrated only on two-pedestrian group data [Eq. (37)] in dashed blue (dark gray); simulation using parameters calibrated on two- and three-pedestrian groups [Eq. (47)] in solid orange (light gray). (b) Same comparison for the angle between the wing pedestrians, θ_{13}.

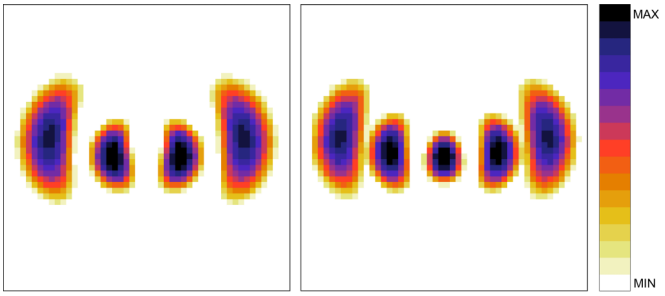

FIG. 14. (Color online) (a) Four- and (b) five-person group *pdf*s (logarithmic plots) obtained using parameters optimized by Eq. (47). Panel (a) shows a 3.5-m-wide area, while panel (b) shows a 4.5-m-wide area.

described by the first-neighbor model as farther apart than they are in the empirical distribution. Such a weak point of the model is confirmed by the poor description of the r_{13} distribution [Fig. 13(a)]. On the contrary, the θ_{13} distribution is very well described and also very well predicted by the model calibrated only on two-pedestrian data [Fig. 13(b)]. The parameters calibrated using Eq. (37) and Eq. (47) provide basically an equivalent description of two-pedestrian groups (Table III), and a quite similar one for three-pedestrian groups, suggesting that the model does not depend very strongly on the specific parameter values.

F. Limitations in the description of three-person groups

The first-neighbor model calibrated on two-pedestrian data [Eq. (37)] could qualitatively and quantitatively describe the most probable configuration and the velocity of the three-pedestrian groups. Furthermore, the quantitative description was significantly improved after calibration on all the available data [Eq. (47)]. According to us, these results show that the main features of the three-pedestrian group dynamics may be described on the basis of our first-neighbor model developed for the two-pedestrian case.

Nevertheless, in an actual fully interacting three-pedestrian group, the pedestrians on the wings are aware of each other, and their presence should affect each other's dynamics. By neglecting this interaction we obtained a good description of the three-person dynamics, showing that the first-neighbor term is the leading one, but the second-neighbor term is definitely present as a perturbation.

The presence of this term is probably the cause of the main deviations of our model from the empirical distributions, which are as follows:

(a) the overestimate of the distance between the pedestrians on the wings, r_{13};

(b) the absence of asymmetry in the θ_{12} distribution; and

(c) the underestimate of the width of the distributions (standard deviations) around maxima.

The first effect could be due to an attractive term between the two pedestrians on the wings, while the second one could be due to the discomfort that the pedestrians on the wings would feel if the central pedestrians hinder their gaze, and thus their communication, with their presence. This term would emerge when $\theta_{12} = -\theta_{32} \approx \pi/2$ and be negligible for lower values of $|\theta|$, leading to the asymmetry in the distribution of Fig. 13(a). Finally, the presence of these perturbing terms could cause the large spreads around the maxima for the empirical three-pedestrian distributions.

VII. LARGER GROUPS

We applied the first-neighbor model to four- and five-person groups, obtaining the results of Fig. 14. Simulated pedestrians walk mostly abreast at a distance of $\approx r_0$ in slightly U bent formations (the central pedestrians on the rear). The velocities are 1.09 m/s for $n = 4$ and 1.08 m/s for $n = 5$.

These results are in agreement with the findings of Ref. [5], provided that, as it happened for three-person groups, bent formations emerge also for unconstrained groups. Furthermore, the result for the four-person group velocity is in agreement with Table I. We also notice that the four-person distribution is quite similar to the one observed by Ref. [4]. This latter work uses short time window observations, and thus their recognition of four-person groups is biased towards groups that are actually *fully interacting at the moment of observation*. Their observations thus suggest that at a time in which all the members of the group are involved in the same conversation, our first-neighbor model correctly describes their interaction.

Nevertheless, our observations, based on longer time windows, suggest that such *full member interactions* are very limited in time for groups with more than three members. Indeed, we have not observed in our environment such U-shaped formations in large groups, or at least they are not stable in the sense of that described in Ref. [14]. In this latter work we analyzed the spatial distribution of four-person interacting groups and verified that they do not present a stable four-person structure like those found for two- and three-person groups.

We found, conversely, that four-person groups present stable two-person subgroups, whose structure resembles the one described by our model. We believe that when they form a two- or three-person subgroup, pedestrians become almost neutral to the interaction with the other

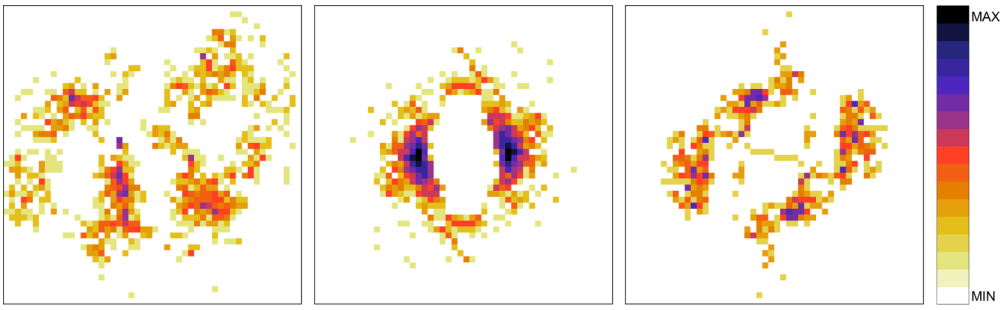

FIG. 15. (Color online) Logarithmic plots for (a) empirical *pdf* for the position of a pedestrian in the center-of-mass frame of a four-person group; (b) empirical *pdf* for the position of a pedestrian in the center-of-mass frame of a two-person subgroup; (c) empirical *pdf* for the position of a two-pedestrian subgroup in the overall four-person group center-of-mass frame. Black indicates maximum probability and white minimum probability. Each area is 2.5 m wide.

members of their group. The inter-sub-group interaction is then described by the same potential used in this paper but perturbed by a weaker interaction term with the other members.

Figure 15(a) shows the center-of-mass reference frame probability distribution for four-person groups, without any stable formation. In Fig. 15(b) we show the probability distribution for two-person subgroups[40] that resembles the distribution generated by our potential. Finally, in Fig. 15(c) we show the distribution for the position of the two subgroups' centers of mass in the overall center-of-mass frame. Such a distribution suggests a weaker θ dependence with minima at $\theta = n\pi/2$, $n = -1,0,1,2$ (the minima for $\pm\pi/2$ appear to be at a slightly higher distance). We leave a mathematical treatment of this potential for future work, considering also the limited amount of four-person groups observed (Table I).

VIII. DISCUSSION AND CONCLUSIONS

In this paper we introduced a simple potential for the discomfort of a pedestrian that is not located in the optimal position for interacting with a walking partner. By assuming that the potential is the sum of a radial term and a quadratic angular term, we obtained a very good description of the probability distribution around the position of maximum comfort (both using the theoretically predicted Boltzmann distribution or using the results of numerical integrations).

In the model we decided to introduce the term η that is not directly observable when studying the two-pedestrian relative distance distribution. This term arises naturally in the formulation of our angular discomfort potential, Eq. (13), as the relative weight that the pedestrians give to the angle that their gaze has to span with respect to the partner's corresponding angle. The simplest hypothesis would be to assume symmetry and put $\eta = 0$. Nevertheless, an $\eta < 0$ value explains, without any other assumption, two of our empirical findings as follows:

(1) Groups are slower than single pedestrians, and the difference in velocity between three-pedestrian and two-pedestrian groups is roughly one-third of the difference between two-pedestrian groups and single pedestrians [Eqs. (29), (43), and (46)].

(2) Three-pedestrian groups walk in a V formation with the central pedestrian on the rear.

We consider these two results the most relevant success of our model.

It is arguable that the cognitive process that leads to these results may differ from the one that led us to Eq. (13): $\eta < 0$ may represent not an asymmetrical preference to walk on the rear and having the partner in the field of view (more than being in the partner's field of view) but a more symmetrical term, as the load of being involved in a conversation, and having the gaze span an angle ψ, causes a slower walking velocity. The good results of our model make us assume that, even if the cognitive process is the latter, our mathematical framework is adequate to describe its main features.

The model can describe the most probable position of pedestrians in two- and three-person groups in 2D space (Figs. 6 and 12). For two-pedestrian groups, the description of the distribution around the maxima is also quite good, and the model only fails in describing the "fat tails" far from equilibrium. Since the hypotheses that led us to the formulation of the model are valid close to equilibrium, this failure appears to be a minor one. For three-pedestrian groups, the description of the distribution around maxima is less precise. In particular, the model seems to fail in describing the asymmetrical distribution of the angle θ_{12} around its most probable value and overestimates the distance between the pedestrians on the wings, r_{13}. As discussed in Sec. VI F, these limitations are probably due to the presence of a three-person specific interaction term between the pedestrians on the wings. In this paper we ignored any such term, assuming that the first-neighbor interaction would be the leading one and would allow us to describe to a good extent the three-person structure based on the two-person one, and

[40] In Ref. [14] we explain the detail of the algorithm for the division in subgroups. Basically, we look for abreast configurations at a 0.75-m distance. We also checked that other ways of dividing the group did not lead to the identification of a stable structure.

our results supported this hypothesis. Nevertheless, including the interaction terms described in Sec. VI F could further improve the ability of our model to reproduce pedestrian behavior.

Possible improvements to the model include a description of the splitting of large groups into subgroups (as mentioned in Sec. VII) and that of the interaction between subgroups, dealing with the three-person-specific terms described in Sec. VI F, and introducing into the model a group-specific collision avoidance behavior that may reproduce the higher-density results of Ref. [5] while obtaining at lower densities the results of the current work. Such a collision avoidance behavior should also take into account the specific behavior of pedestrians *towards* groups.

ACKNOWLEDGMENTS

We are grateful to the Osaka city government, the Osaka Urban Industry Promotion Center, and Osaka Shigaichi Kaihatsu for their support, which made this work possible. A special thank goes to Kanako Tomita and Sayaka Taniguchi for the time and energy consuming labeling work. We also thank Yoshihiro Chigodo, Takahiro Adachi, Kōtarō Hayashi, Kyuhee Lee, and Daniel Rea for help in data collection experiments, and Zeynep Yücel for reading the manuscript and providing useful comments. Finally, we thank the anonymous reviewers whose comments helped us to improve our paper.

APPENDIX A: DEFINITION OF STATISTICAL OBSERVABLES

When talking about statistical properties of a two- or three-body system we necessarily adopt an ergodic point of view, in which physical observables (basically, in the scope of this paper, the position probability distribution)[41] are determined by time integrals

$$\bar{f} = \lim_{T\to+\infty} \frac{\int_0^T f(t)dt}{T}. \tag{A1}$$

Nevertheless, obviously our real-world observations are not based on a single pedestrian pair followed for an infinite time but on N pedestrian pairs followed for finite time, such that the observables are given by

$$\langle f\rangle = \sum_{k=1}^{N} \frac{\int_0^{T_k} f_k(t)dt}{T_k N}, \tag{A2}$$

with finite N and observation times T_k. When we claim that $\boldsymbol{\Xi}$ may be treated as a white noise, we mean that when studied over a $\sum_k T_k$ time scale its distribution can be approximated by a random one. We also note that we cannot assume all pedestrians to behave in the same way, and the interaction force $\mathbf{F}$ will be, in general, pedestrian dependent. Still, if the pedestrian behavior parameters are considered normally distributed, we may include their effect in the term $\boldsymbol{\xi}$ of Eq. (1) [and thus in $\boldsymbol{\Xi}$ of Eq. (4)] and assume that our observations Eq. (A2) are given by Eq. (A1) for the dynamical system of Eq. (4).

APPENDIX B: INDEPENDENCE OF θ AND r

When introducing the full form of the potential D, Eq. (17), we assumed the independence of the variables θ and r. We analyzed the linear correlation index between the angle $-\pi < \theta \leqslant 0$ that gives the position of the pedestrian on the left with respect to the center of mass in a two-pedestrian group (here left is defined with respect to the y axis aligned with $\hat{\mathbf{g}}$), and the distance r, as

$$I_c = \frac{\langle \theta r\rangle - \langle\theta\rangle\langle r\rangle}{\sqrt{\langle\theta^2\rangle - \langle\theta\rangle^2}\sqrt{\langle r^2\rangle - \langle r\rangle^2}}, \tag{B1}$$

and there was no significant linear correlation ($I_c = 0.0007$). To investigate a possible nonlinear dependence between the variables, we computed the mutual information and joint entropy of the θ and r distributions. We discretized the variables in uniform cells and computed the empirical probability distributions $\rho(\theta_i)$, $\rho(r_i)$, and $\rho(\theta_i,r_j)$;[42] the mutual information is given by

$$I(\Theta;R) = \sum_{i,j\in\text{cells}} \rho(\theta_i,r_j)\log_2\left(\frac{\rho(\theta_i,r_j)}{\rho(\theta_i)\rho(r_j)}\right), \tag{B2}$$

while the joint entropy is given by

$$H(\Theta,R) = -\sum_{i,j\in\text{cells}} \rho(\theta_i,r_j)\log_2\left(\rho(\theta_i,r_j)\right). \tag{B3}$$

The Jaccard distance

$$D(\Theta,R) = \frac{H(\Theta,R) - I(\Theta;R)}{H(\Theta,R)}, \tag{B4}$$

which would have a value of 1 for uncorrelated variables, assumes $D(\Theta,R)\approx 0.99$ with extremely weak dependence on the chosen discretization steps. For a result obtained with a different tracking method and in a different cultural context, see the (r,θ) distribution in Ref. [48].

APPENDIX C: THERMAL CORRECTIONS TO THE TWO-PERSON GROUP VELOCITY

To estimate the two-pedestrian group velocity in Eq. (29) we assumed the system to be at zero temperature and thus the center-of-mass acceleration to be directed along $\hat{\mathbf{g}}$. We may, nevertheless, evaluate the average force along y for nonzero

[41] In this work we deal mainly with discretized version of *pdf*s. For example, the probability density for the distance between two pedestrians $\rho(r)$ is approximated by $P(r,\Delta r)$, the probability of the distance to assume values between $r-\Delta r/2$ and $r+\Delta r/2$. The computation of P involves time integrals (or better summations over discrete times) of the characteristic function $\chi(r,\Delta r)$ in the form of Eqs. (A1) or (A2).

[42] Strictly speaking, ρ is a probability and not a *pdf*.

TABLE IV. Agreement between the two coders on pedestrians being or not part of a group. The ratio of pedestrians in groups over all pedestrians was ≈0.19.

	$A=0$	$A=1$
$B=0$	9562	45
$B=1$	365	2227

TABLE V. Cohen κ coefficient [Eq. (D1)] and agreement rate P_a for pedestrian groups being coded as *fully connected socially interacting* by the coders.

	$n=2$	$n=3$	$n=4$
κ	0.62	0.63	0.62
P_a	0.89	0.86	0.81

temperature recalling Eq. (24) and using

$$\overline{F}_y = 4C_\theta\varphi\frac{\int_0^\pi d\theta\int_0^{+\infty} dr\,\sin\theta\, e^{-\frac{U(r,\theta)}{T_\Xi}}}{\int_0^\pi d\theta\int_0^{+\infty} dr\, r\, e^{-\frac{U(r,\theta)}{T_\Xi}}}. \tag{C1}$$

We may expect the correction to Eq. (29) to be a power series in the adimensional temperature terms $T_\Xi/(4C_\theta)$ and $T_\Xi/(2C_r)$ of Eq. (32). According to the analysis of Sec. IV, C_r is one order of magnitude higher than C_θ, so we may expect the angular integral to give the strongest correction. This integral may be solved assuming $\sqrt{T_\Xi/(4C_\theta)} \ll \pi/2$. Changing variable to $\theta' = \theta - \pi/2$ and setting $a = T_\Xi/(4C_\theta)$ we have

$$\frac{\int_0^\pi d\theta\ \sin\theta\ e^{-\frac{U(r,\theta)}{T_\Xi}}}{\int_0^\pi d\theta\ e^{-\frac{U(r,\theta)}{T_\Xi}}} \approx I_\theta \equiv (2\pi a)^{-\frac{1}{2}}\int_{-\infty}^{+\infty} d\theta'\cos\theta' e^{-\frac{\theta'^2}{2a}}. \tag{C2}$$

Expanding $\cos\theta'$ as a power series and using the Gaussian integral formula, we get

$$\begin{aligned} I_\theta &= \sum_{n=0}^{\infty}(-)^n\frac{(2n-1)!!}{2n!}a^n = \sum_{n=0}^{\infty}\frac{1}{(2n)!!}(-a)^n \\ &= \sum_{n=0}^{\infty}\frac{1}{n!}\left(\frac{-a}{2}\right)^n = e^{-\frac{a}{2}}, \end{aligned} \tag{C3}$$

where we used the relation $(2n)!! = 2^n n!$. We may use Eq. (C3) [or a numerical estimate of Eq. (C1)] in place of Eq. (29) to estimate η as we did in Sec. IV C. We find values of $\eta^{\text{analytic}} = -0.214$ using Eq. (C3) and $\eta^{\text{numerical}} = -0.22$ using the numerically computed value of Eq. (C1). When these η values are used in the simulator of Sec. V we obtain average values of $\overline{V}_y^{\text{analytic}} = 1161$ mm/s and $\overline{V}_y^{\text{numerical}} = 1156$ mm/s, showing agreement between the analytical results of Sec. IV and the numerical ones of Sec. V.

We nevertheless notice that for these numerically integrated systems, the average center-of-mass velocity $\overline{V}$ was ≈1170 mm/s due to the effect of a nonzero $\overline{V}_x^2$ component at nonzero temperature. Given our operational definition of empirical observables [Eq. (34)], only the average velocity $\overline{V}$ is observable for actual pedestrian groups, while our estimates for the group velocities based on Eqs. (29), (43), (46), (C1), and (C3) are more properly given for the average velocity in the goal direction. Nevertheless, as discussed above, by numerically integrating the three-pedestrian system we find a difference between $\overline{V}$ and $\overline{V}_y$ which is of the order of magnitude of the standard error of the measurement of pedestrian group velocity, confirming that Eqs. (29), (43), and (46) may be used to obtain a reliable estimate of group velocities.[43]

APPENDIX D: CODERS AGREEMENT

Table IV shows the number of pedestrians coded as members of groups by both coders (A and B), $n_{A=1,B=1}$; by none of them, $n_{A=0,B=0}$; or those on which they disagree, $n_{A=1,B=0}$ and $n_{A=0,B=1}$.[44]

To evaluate the quality of the agreement between coders, we may use the Cohen's κ coefficient. If P_a is the agreement rate, and P_{ra} the probability of random agreement, the coefficient is defined as

$$\kappa = \frac{P_a - P_{\text{ra}}}{1 - P_{\text{ra}}}. \tag{D1}$$

For the data of Table IV we have $P_a = 0.97$ and $\kappa = 0.895$ (Ref. [49] considers $0.6 < \kappa \leqslant 0.8$ as substantial agreement, and $\kappa > 0.8$ as almost perfect). Table V shows the κ and P_a values for groups being coded as fully interacting or not by the coders.

APPENDIX E: EULER INTEGRATOR

Equation (4) is discretized as

$$\begin{aligned} \mathbf{v}(t+\Delta t) &= \mathbf{v}(t) + (\mathbf{F}_{\text{ns}}(\mathbf{x}(t),\mathbf{v}(t)) + \boldsymbol{\Xi}(t))\Delta t, \\ \mathbf{x}(t+\Delta t) &= \mathbf{x}(t) + \mathbf{v}(t+\Delta t)\Delta t, \end{aligned} \tag{E1}$$

where $\mathbf{F}_{\text{ns}}$ includes all nonstochastic acceleration terms.

[43] Assuming thermal corrections to be small, and more or less equivalent for the two- and three-pedestrian groups, we understand the validity of Eq. (46). This latter equation is almost exact if thermal corrections in three-person groups are ≈4/3 times the two-person corrections.

[44] Over $N = 12\,199$ pedestrians on 9 h of data.

[1] J. Coleman and J. James, Sociometry **24**, 36 (1961).
[2] J. James, American Sociological Review **18**, 569 (1953).
[3] A. F. Aveni, Sociometry **40**, 96 (1977).
[4] M. Schultz, L. Rößger, H. Fricke, and B. Schlag, in *Pedestrian and Evacuation Dynamics 2012*, edited by U. Weidmann, U. Kirsch, and M. Schreckenberg (Springer, Berlin, 2014), Vol. II, pp. 1097–1111.
[5] M. Moussaïd, N. Perozo, S. Garnier, D. Helbing, and G. Theraulaz, PLoS ONE **5**, e10047 (2010).
[6] L. Manenti, S. Manzoni, G. Vizzari, K. Ohtsuka, and K. Shimura, in *Multi-Agent-Based Simulation XII* (Springer, Berlin, 2012), pp. 74–89.
[7] S. Xu and H.-L. Duh, IEEE Trans. Intell. Transp. Syst. **11**, 153 (2010).
[8] G. Köster, M. Seitz, F. Treml, D. Hartmann, and W. Klein, Contemp. Soc. Sci. **6**, 397 (2011).
[9] I. Karamouzas and M. Overmars, in *Proceedings of the 17th ACM Symposium on Virtual Reality Software and Technology* (ACM, New York, 2010), pp. 183–190.
[10] Y. Zhang, J. Pettré, X. Qin, S. Donikian, and Q. Peng, in *12th International Conference on Computer-Aided Design and Computer Graphics (CAD/Graphics), 2011* (IEEE, Jinan, China, 2011), pp. 275–281.
[11] E. Hall, *The Hidden Dimension* (Anchor Books, New York, 1969).
[12] A. Kendon, *Conducting Interaction: Patterns of Behavior in Focused Encounters* (Cambridge University Press, Cambridge, 1990), Vol. 7.
[13] M. Costa, J. Nonverb. Behav. **34**, 15 (2010).
[14] F. Zanlungo and T. Kanda, in *COGSCI13* (Cognitive Science Society, Austin, TX, 2013).
[15] C. Castellano, S. Fortunato, and V. Loreto, Rev. Mod. Phys. **81**, 591 (2009).
[16] L. Henderson, Nature **229**, 381 (1971).
[17] P. P. Kachroo, S. J. Al-Nasur, and S. A. Wadoo, *Pedestrian Dynamics: Feedback Control of Crowd Evacuation* (Springer, Berlin, 2008).
[18] M. Muramatsu and T. Nagatani, Physica A **286**, 377 (2000).
[19] C. Burstedde, K. Klauck, A. Schadschneider, and J. Zittartz, Physica A **295**, 507 (2001).
[20] M. Schultz and H. Fricke, in *Cellular Automata* (Springer, Berlin, 2010), pp. 506–512.
[21] D. Helbing and P. Molnar, Phys. Rev. E **51**, 4282 (1995).
[22] D. Helbing, P. Molnar, I. Farkas, and K. Bolay, Environ. Plann. B **28**, 361 (2001).
[23] S. Hoogendoorn and W. Daamen, Traffic Granul. Flow **03**, 373 (2005).
[24] T. Kretz, A. Grünebohm, M. Kaufman, F. Mazur, and M. Schreckenberg, J. Stat. Mech.: Theor. Exp. (2006) P10001.
[25] D. Helbing and A. Johansson, Encycl. Complex. Syst. Sci. **16**, 6476 (2009).
[26] F. Zanlungo, T. Ikeda, and T. Kanda, Europhys. Lett. **93**, 68005 (2011).
[27] G. Turchetti, F. Zanlungo, and B. Giorgini, Europhys. Lett. **78**, 58003 (2007).
[28] A. Sud, E. Andersen, S. Curtis, M. C. Lin, and D. Manocha, IEEE Trans. Vis. Comput. Graphics **14**, 526 (2008).
[29] J. Ondřej, J. Pettré, A. Olivier, and S. Donikian, ACM Transact. Graphic. **29**, 123 (2010).
[30] M. Moussaïd, D. Helbing, S. Garnier, A. Johansson, M. Combe, and G. Theraulaz, Proc. R. Soc. B: Biol. Sci. **276**, 2755 (2009).
[31] S. J. Guy, S. Curtis, M. C. Lin, and D. Manocha, Phys. Rev. E **85**, 016110 (2012).
[32] A. Johansson, D. Helbing, and P. K. Shukla, Adv. Complex Syst. **10**, 271 (2007).
[33] C. McPhail and R. T. Wohlstein, Sociol. Methods Res. **10**, 347 (1982).
[34] M. L. Knapp, *Nonverbal Communication in Human Interaction* (Cengage Learning, Stamford, CT, 2012).
[35] C. L. Kleinke, Psychol. Bull. **100**, 78 (1986).
[36] M. Argyle and J. Dean, Sociometry **28**, 289 (1965).
[37] Z. Yücel, F. Zanlungo, T. Ikeda, T. Miyashita, and N. Hagita, Sensors **13**, 875 (2013).
[38] J. Zacharias, J. Environ. Psychol. **21**, 341 (2001).
[39] S. P. Hoogendoorn and P. H. Bovy, Transport. Res. B Methodol. **38**, 169 (2004).
[40] T. Kretz, J. Stat. Mech.: Theor. Exp. (2009) P03012.
[41] S. Thompson, T. Horiuchi, and S. Kagami, in *Proceedings of the 13th IASTED International Conference on Robotics and Applications of RA '07* (ACTA Press Anaheim, CA, USA, 2007), pp. 119–125.
[42] S. Hoogendoorn and P. HL Bovy, Optim. Contr. Appl. Methods **24**, 153 (2003).
[43] F. Zanlungo, T. Ikeda, and T. Kanda, PloS ONE **7**, e50720 (2012).
[44] F. Zanlungo, Y. Chigodo, T. Ikeda, and T. Kanda, in *Pedestrian and Evacuation Dynamics 2012*, edited by U. Weidmann, U. Kirsch, and M. Schreckenberg (Springer, Berlin, 2014), Vol. I, pp. 289–304.
[45] sites.google.com/site/francescozanlungo/pedestriandata
[46] D. Glas, T. Miyashita, H. Ishiguro, and N. Hagita, Adv. Robot. **23**, 405 (2009).
[47] N. Saunier, A. El Husseini, K. Ismail, C. Morency, J.-M. Auberlet, and T. Sayed, Transp. Res. B **2264**, 138 (2011).
[48] S. Pellegrini, A. Ess, and L. Van Gool, in *Computer Vision–ECCV 2010* (Springer, Berlin, 2010), pp. 452–465.
[49] J. R. Landis and G. G. Koch, Biometrics **33**, 159 (1977).